

Elucidating the mechanism of perovskite surface passivation with organic molecules: the impact of π -conjugation length

Daichi Koseki,^{abc} Chathuranganie A. M. Senevirathne,^a Dai Senba,^{ad} Yuki Fujita,^{ab} Jun Lin,^{ad} Mengde Zhai,^{ade} Juan Shang,^a Telugu Bhim Raju,^a Shintaro Ida,^{fg} Motonori Watanabe,^{abdg} Aleksandar Staykov,^{abg} Hiroshi Segawa,^{ch} Zhanglin Guo,^{adg} Toshinori Matsushima^{*abdg}

^a *International Institute for Carbon-Neutral Energy Research (WPI-I2CNER), Kyushu University, Fukuoka 819-0395, Japan. E-mail: tmatusim@i2cner.kyushu-u.ac.jp*

^b *Department of Applied Chemistry, Faculty of Engineering, Kyushu University, Fukuoka 819-0395, Japan.*

^c *Department of General Systems Studies, Graduate School of Arts and Sciences, The University of Tokyo, Tokyo 153-8902, Japan.*

^d *Department of Automotive Science, Graduates School of Integrated Frontier Sciences, Kyushu University, 744 Motoooka, Nishi, Fukuoka 819-0395, Japan*

^e *Institute for Energy Research, School of Energy and Power Engineering, Jiangsu University, Zhenjiang 212013, China*

^f *Institute of Industrial Nanomaterials (IINa), Kumamoto University, Kumamoto 860-8555, Japan.*

^g *Center for Energy Systems Design (CESD), International Institute for Carbon-Neutral Energy Research (WPI-I2CNER), Kyushu University, Fukuoka 819-0395, Japan*

^h *Research Center for Advanced Science and Technology, The University of Tokyo, Tokyo 153-8904, Japan*

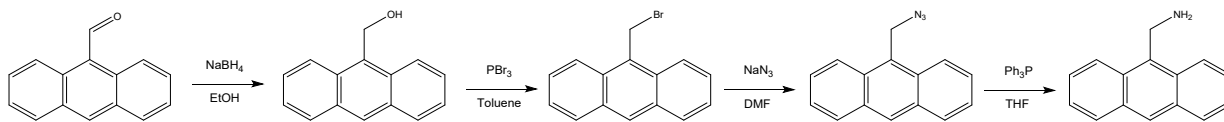


Figure S1. Synthetic pathway to obtain AMA.

Synthesis of 9-bromomethyl anthracene^{S1,S2}

9-Anthraldehyde (5.0 g, 24.2 mmol) in ethanol (30 mL) was added slowly a mixture of NaBH₄ (2.5 g, 66 mmol) at 0 °C. After stirring for 2 h, water was poured into the mixture. After filtration, light yellow solid (4.8 g) was obtained. This compound was used for the next step without further purification.

9-Anthracenemethanol (4.8 g, 23.1 mmol) in dried toluene (200 mL) was slowly added PBr₃ (5 mL). The reaction mixture was stirred for 1 h at 0 °C and then stirred for 1 h at room temperature. The reaction mixture was quenched with NaHCO₃. The organic phase was extracted with toluene, washed with water, and combined organic phase was dried over MgSO₄. The residue was concentrated to afford 9-bromomethyl anthracene as a yellow solid. (4.6 g, 70% in two steps).

¹H NMR (400 MHz, CDCl₃): δ 8.50 (s, 1H), 8.31 (d, 2H, J = 8.8 Hz), 8.05 (d, 2H, J = 8.4 Hz), 7.67–7.63 (m, 2H), 7.53–7.49 (m, 2H), 5.55 (s, 2H)

Synthesis of 9-aminomethyl anthracene^{S3}

9-Bromomethyl anthracene (4.6 g, 17.0 mmol) was dissolved in dried DMF (125 mL) and sodium azide (4.42 g, 68.0 mmol). The reaction was then heated to 50 °C and stirred for 1 h under N₂ atmosphere. The reaction mixture was cooled to room temperature then poured into water. The reaction mixture was extracted with ether, then organic layer was washed with brine, and dried with MgSO₄. The residue was concentrated to afford 9-azidomethyl anthracene as a yellow solid. (3.3 g). This compound was used for the next step without further purification.

9-Azidomethyl anthracene (3.3g, 14.2 mmol) in dried THF (25 mL) was added triphenylphosphine (4.1 g, 15.6 mmol) at 0 °C under nitrogen atmosphere. The reaction was stirred for 6 h at 0 °C under nitrogen atmosphere. After the reaction, then allowed increase at room temperature while being allowed to warm to room temperature, water was slowly added 1.6 mL followed by an additional hour of stirring at room temperature. After the reaction, ether was added, and the solution cooled to 0 °C. 10% aq. HCl (16 mL) was slowly added into the reaction mixture, and precipitation of the amine hydrochloride salt that was filtered and washed with minimal cold 50% aq. acetone solution. The amine hydrochloride salt was dissolved with ethyl acetate, neutralized with excess NH₃ solution. The resultant solution was extracted with ethyl acetate, then the organic layer was washed with brine, and dried with Na₂SO₄. The residue was concentrated to afford 9-aminomethyl anthracene as a yellow solid. (1.4 g, 48% in two steps).

¹H NMR (400 MHz, CDCl₃) δ 8.40 (s, 1H), 8.34 (d, J = 8.8 Hz, 2H), 8.02 (d, J = 8.4 Hz, 2H), 7.57–7.45 (m, 4H), 4.83 (s, 2H).

¹³C NMR (100 MHz, CDCl₃) δ 134.65, 131.74, 129.37, 129.31, 126.93, 126.15, 124.99, 123.74, 38.29.

[S1] Dong, J.; Liu, W.; Ying, S.; Wu, Y.; Xue, S.; Yang, W. *J. Lumin.* **2016**, *176*, 168–174.

[S2] Ju H.; Hiraoka, T.; Horita, H.; Lee, E.; Ikeda, M.; Kuwahara, S.; Habata, Y. *Dalton Trans.* **2022**, *51*, 15530–15537.

[S3] Sims, M. B.; Lessard, J. J.; Bai, L.; Sumerlin, B. S. *Macromolecules*, **2018**, *51*, 6380–6386.

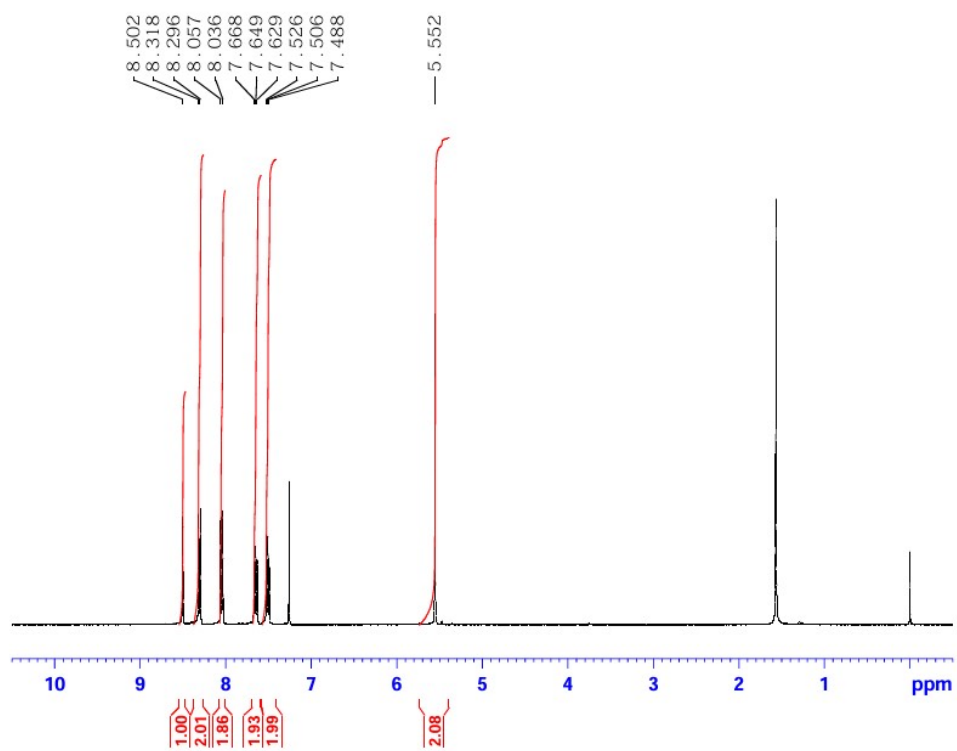


Figure S2. ^1H NMR of 9-bromomethyl anthracene.

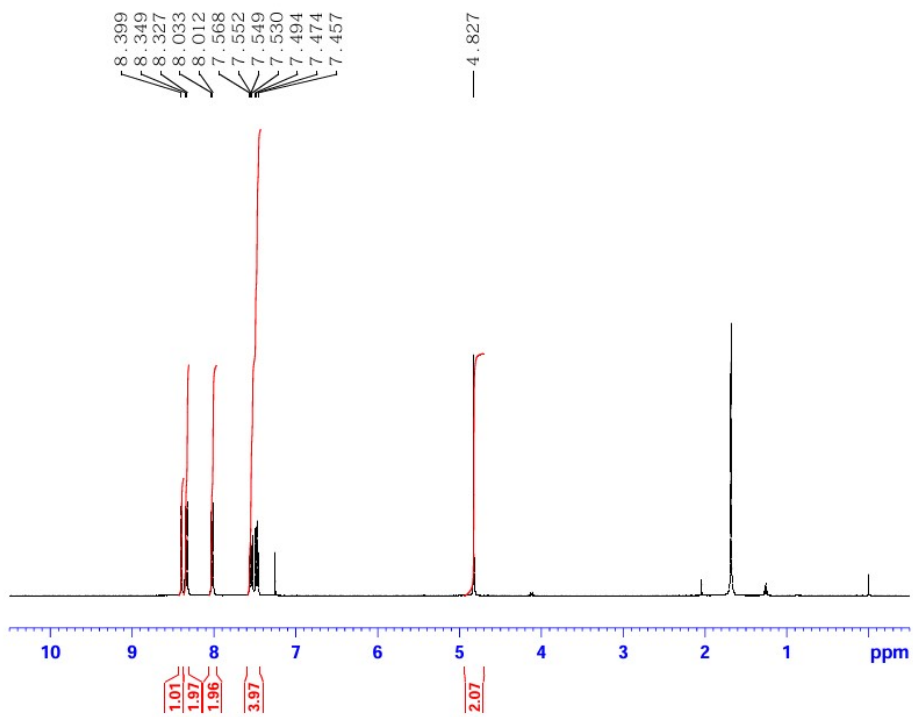


Figure S3. ^1H NMR of 9-aminomethyl anthracene.

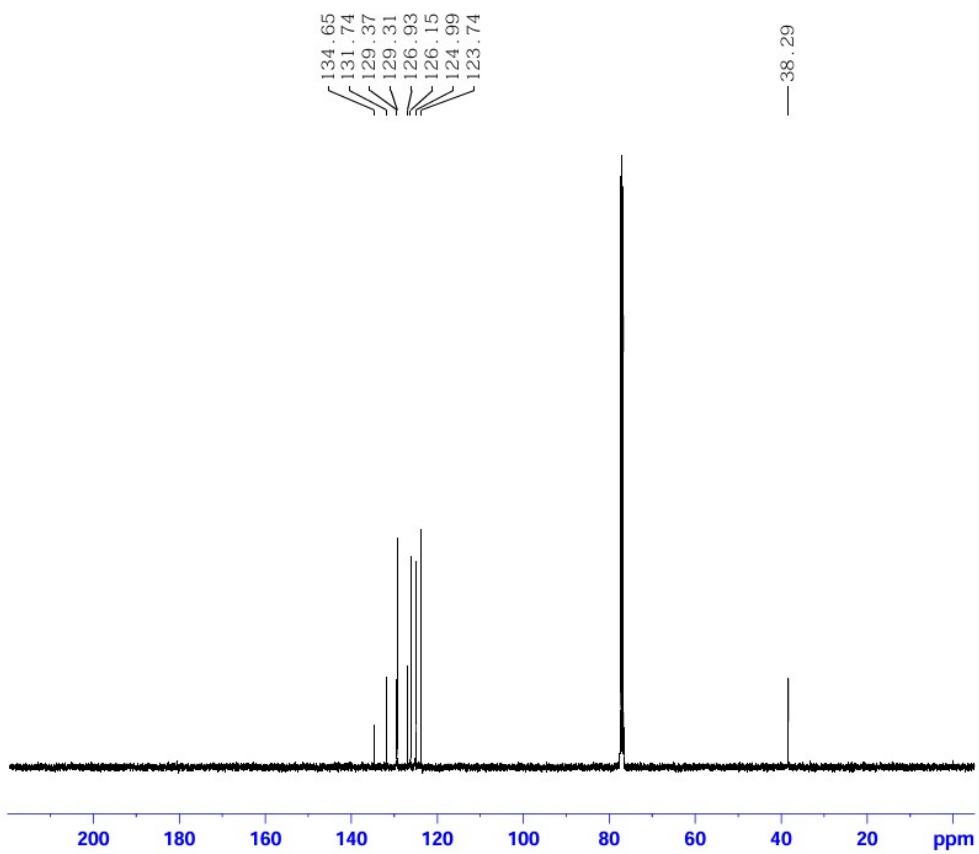


Figure S4. ^{13}C NMR of 9-aminomethyl anthracene.

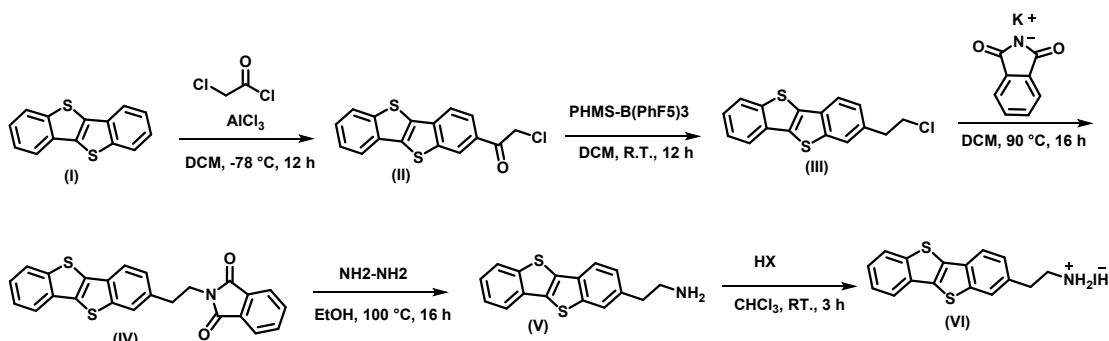


Figure S5. Synthetic pathway to obtain BTBTAl.

Synthesis of 1-(benzo[*b*]benzo[4,5]thieno[2,3-*d*]thiophen-2-yl)-2-chloroethan-1-one (II)

I (1 g, 4.16 mmol) was dissolved in dry DCM (150 mL) under a N₂ atmosphere and cooled to 10 °C. Then, the reaction mixture was cooled to -78 °C and AlCl₃ (0.55 g, 4.16 mmol) was added. Next, 3-chloroethanoyl chloride (0.5 mL, 4.16 mmol) was added drop-wise and the mixture was stirred for 4 h and allowed to warm up till room temperature. The reaction was then quenched with ice water and diluted with MeOH, causing the precipitation of the product. The product was filtered off, washed with water (2 × 50 mL) and MeOH (2 × 50 mL) and dried under vacuum. This product was used for the next step without further purification.

Synthesis of 2-(2-chloroethyl)benzo[*b*]benzo[4,5]thieno[2,3-*d*]thiophene (III)

To a solution of carbonyl compound II (1 mmol) in dry DCM (15 mL) and tris (pentafluorophenyl)borane (5 mol%) was slowly added polymethylhydrosiloxane (3 mmol) at room temperature. The mixture was stirred for 12 h. The residue was purified by column chromatography (hexane:CHCl₃ = 10:2), to obtain III as an off-white solid (yield= 60 %). ¹H NMR (600 MHz, CDCl₃) δ 7.91 (dd, 1H), 7.89 – 7.85 (m, 1H), 7.84 – 7.77 (m, 1H), 7.72 (d, 1H), 7.46 (t, 1H), 7.42 – 7.37 (m, 1H), 7.27 (dd, 1H), 3.79 (t, 2H), 3.20 (d, 2H). ¹³C NMR (151 MHz, CDCl₃) δ 142.72, 142.28 (s), 140.87, 135.27, 135.13, 134.05, 133.45 – 132.73, 132.01, 126.03, 125.37 – 124.78, 124.15, 121.72, 77.37, 77.16, 76.95, 45.12, 39.27.

Synthesis of 2-(2-(benzo[*b*]benzo[4,5]thieno[2,3-*d*]thiophen-2-yl)ethyl)isoindoline-1,3-dione (IV)

Potassium 1,3-dioxoisindolin-2-ide (0.67 g, 2.12 mmol) and III (0.49 g, 2.65 mmol) were dissolved in DMF (10 mL), heated to 90 °C and stirred for 16 h. After the reaction was completed, aqueous NH₄Cl was added and the reaction mixture was extracted with CHCl₃ (3 × 50 mL). Then, the organic layers were combined and dried with magnesium sulphate, filtered and the solvent was evaporated under reduced pressure. The residue was recrystallized from MeOH to obtain IV as an off-white solid (yield= 65 %). ¹H NMR (600 MHz, CDCl₃) δ 7.91 (d, 1H), 7.87 – 7.80 (m, 4H), 7.75 (s, 1H), 7.68 (dd, 2H), 7.44 (t, 1H), 7.39 (dd, 1H), 7.33 (dd, 1H), 4.03 – 3.97 (m, 2H), 3.18 – 3.11 (m, 2H). ¹³C NMR (151 MHz, CDCl₃) δ 168.33, 142.34, 140.69, 135.08, 134.07, 133.93, 133.47, 133.21, 132.12, 126.20, 125.11, 124.96, 124.19, 123.39, 121.94 – 121.58, 77.37, 77.16, 76.95, 39.52, 34.72.

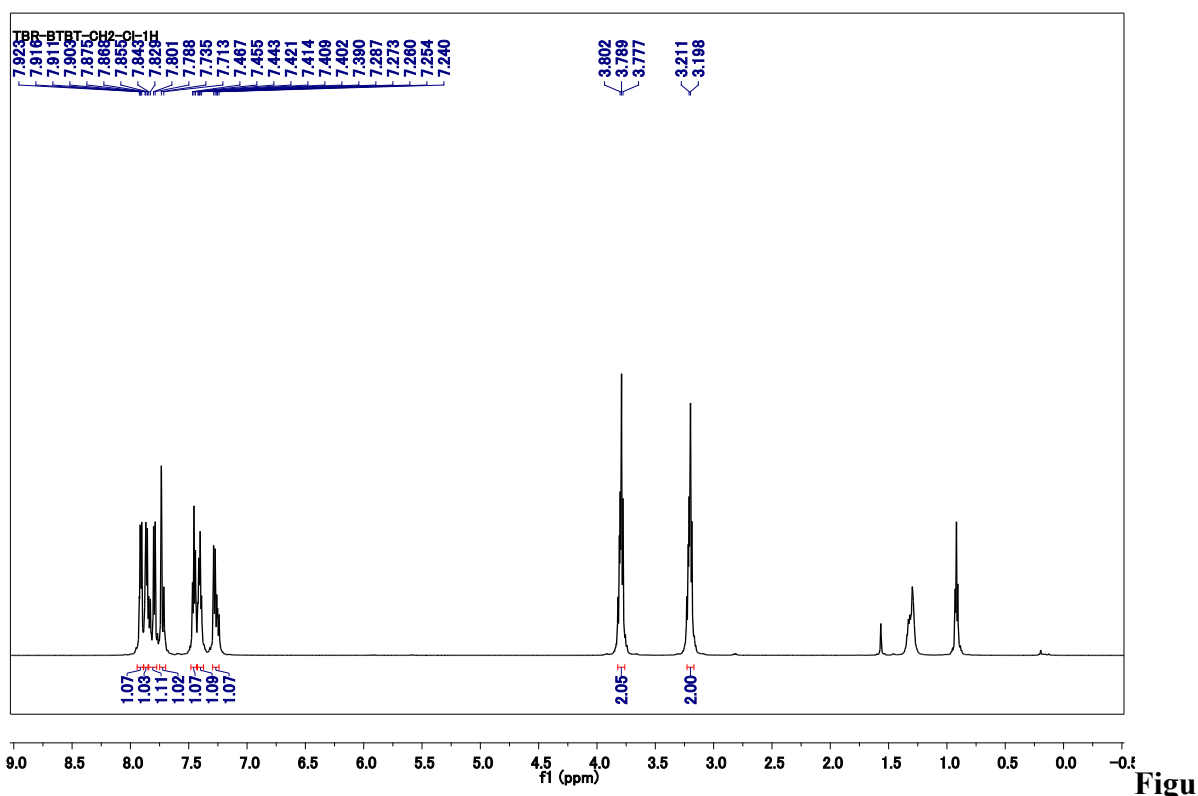
Synthesis of 2-(benzo[*b*]benzo[4,5]thieno[2,3-*d*]thiophen-2-yl)ethan-1-amine (V)

Hydrazine monohydrate (65 wt. % in H₂O, 8.2 mL, 85.2 mmol) was added to a refluxing solution of V (1 g, 4.91 mmol) in EtOH (75 mL) and reacted overnight. Over the course of the reaction, large white crystals precipitate. After the reaction was completed, the reaction mixture was allowed to cool down to room temperature and the precipitate was filtered off and the solvent was evaporated under reduced pressure. Next, the residue was dissolved in CHCl₃ and again filtered. The filtrate was concentrated by rotary evaporation. Afterwards, basic water (pH

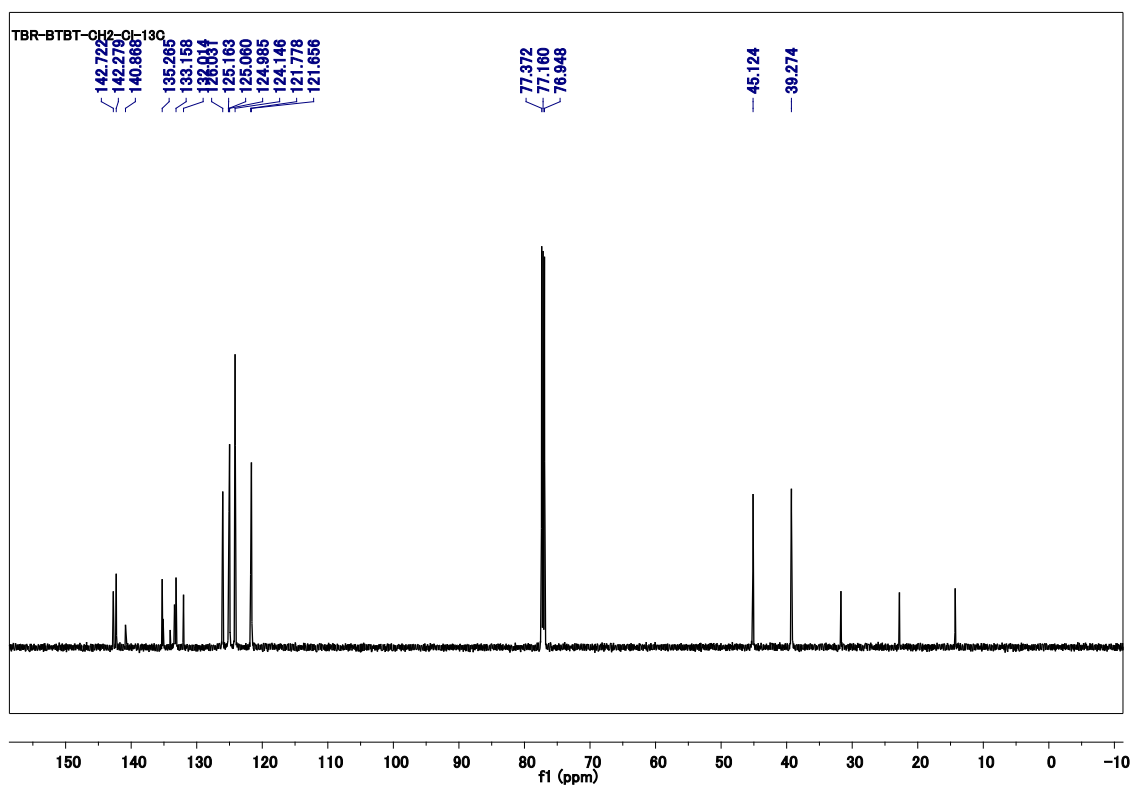
= 12, 50 mL) and CHCl_3 were added and the mixture was extracted with CHCl_3 (2×50 mL). Then, the organic layer was dried with magnesium sulphate, filtered and the solvent was evaporated under reduced pressure to obtain V as an off-white solid (yield= 90 %). ^1H NMR (600 MHz, CDCl_3) δ 7.91 (d, 1H), 7.87 (d, 1H), 7.81 (d, 1H), 7.75 (s, 1H), 7.45 (t, 1H), 7.39 (t, 1H), 7.31 (s, 1H), 3.06 (t, 2H), 2.90 (t, 2H), 1.31 – 1.02 (m, 2H). ^{13}C NMR (151 MHz, CDCl_3) δ 142.80, 142.24, 137.32, 133.35, 133.00, 131.59, 126.23, 124.98, 124.10, 121.62, 77.37, 77.16, 76.95, 43.84, 40.35.

Synthesis of 2-(benzo[b]benzo[4,5]thieno[2,3-d]thiophen-2-yl)ethan-1-amine, hydroiodide (VI)

Hydroiodic acid (HI, 57 % w/w) was added to a solution of V (500.0 mg, 1.68 mmol) in CHCl_3 at room temperature. The salt precipitates from the reaction mixture. Afterwards, the precipitate was filtered. Next, the precipitate was redissolved in EtOH and precipitated in a large amount of cooled ether. The precipitate was further purified by recrystallization in EtOH to obtain VI as an off white solid (yield = 90%). ^1H NMR (600 MHz, DMSO) δ 8.16 (d, J = 8.0 Hz, 1H), 8.05 (dd, J = 13.7, 2H), 7.83 (s, 2H), 7.54 (t, 1H), 7.51 – 7.47 (m, 1H), 7.44 (d, J = 8.1 Hz, 1H), 3.37 (m, 8H), 3.17 (d, 2H), 3.09 – 3.00 (m, 2H). ^{13}C NMR (151 MHz, CDCl_3) δ 142.03, 141.56, 135.08, 132.72, 132.63, 132.43, 131.21, 126.56, 125.51, 124.33, 121.98, 121.80, 121.62, 48.65, 33.02.

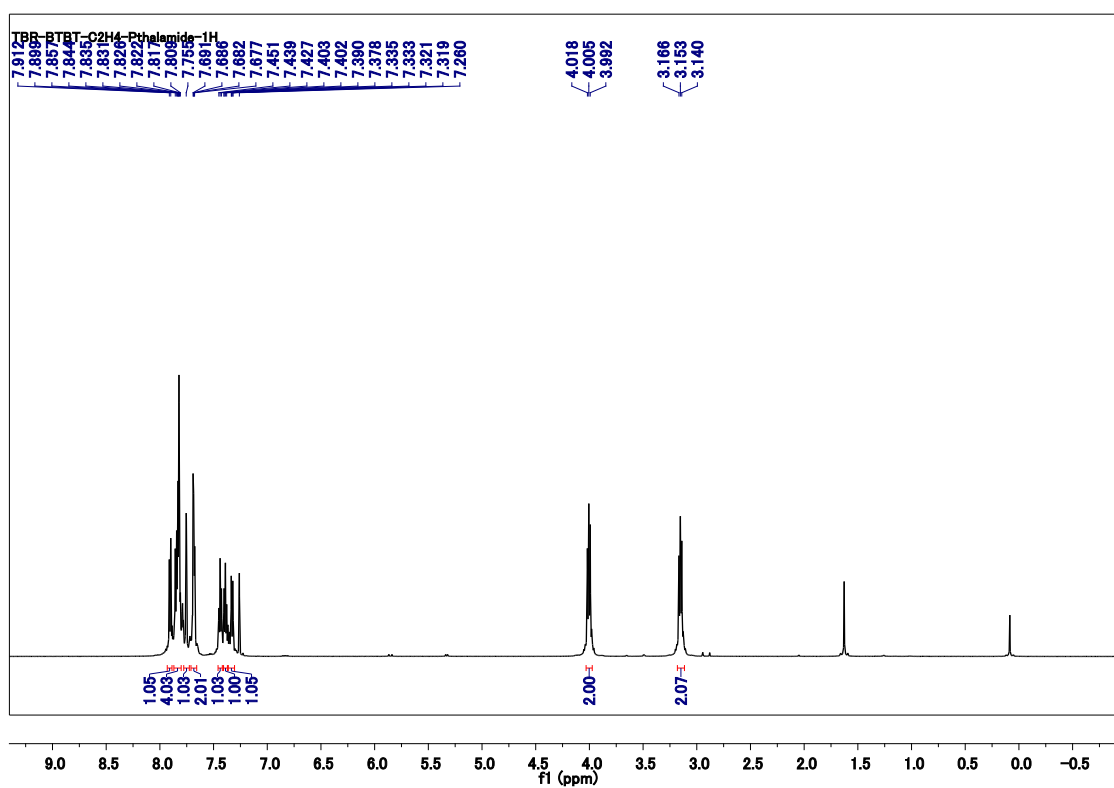


re S6. ^1H NMR spectrum of III in deuterated chloroform.



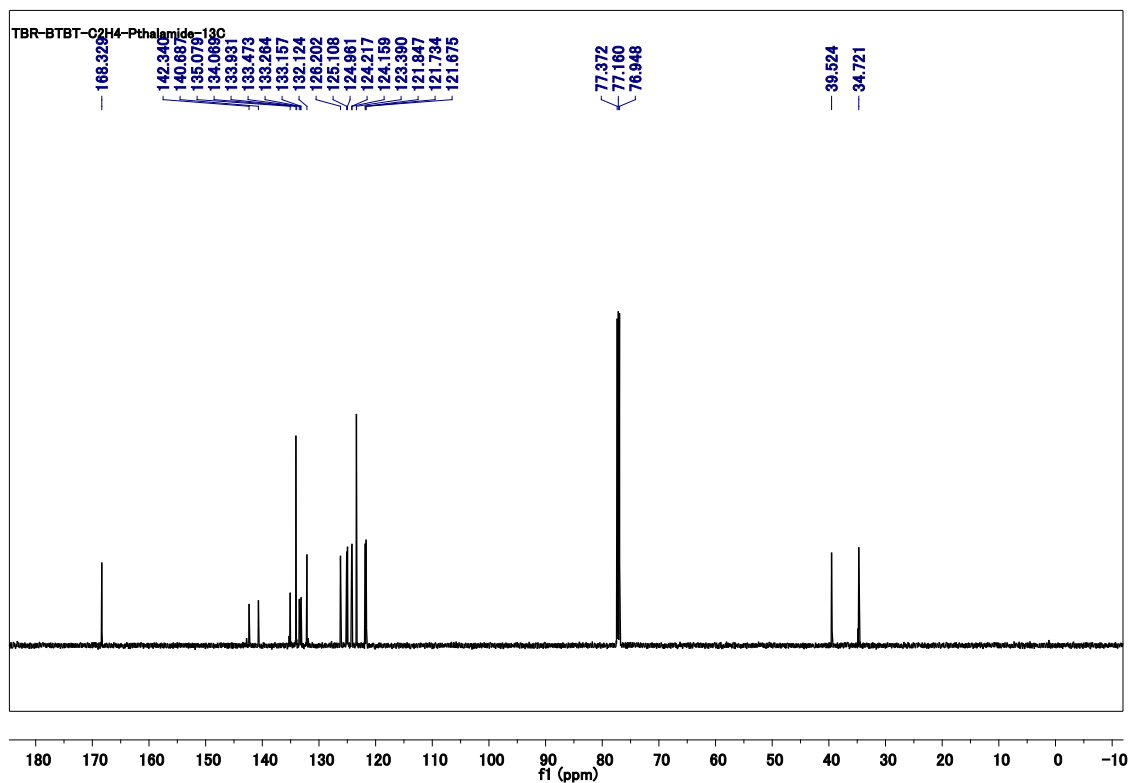
re S7. ¹³C NMR spectrum of III in deuterated chloroform.

Fig



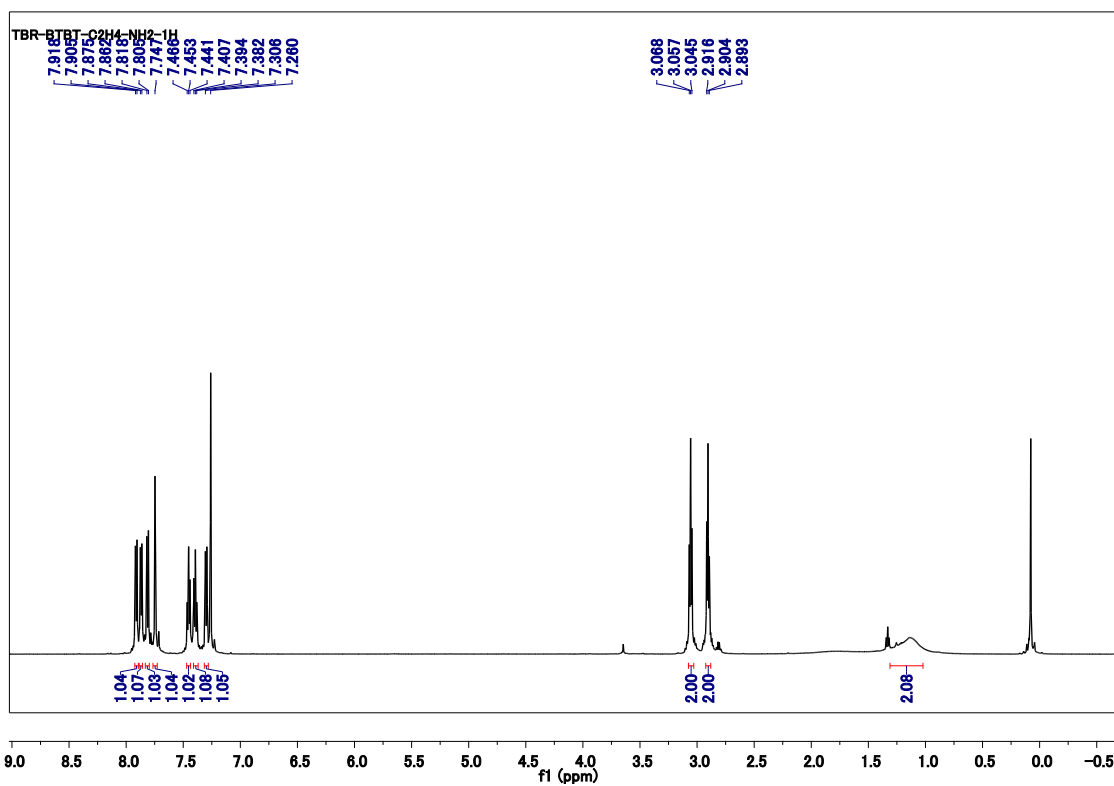
re S8. ¹H NMR spectrum of IV in deuterated chloroform.

Fig



re S9. ^{13}C NMR spectrum of IV in deuterated chloroform.

Fig



re S10. ^1H NMR spectrum of V in deuterated chloroform.

Fig

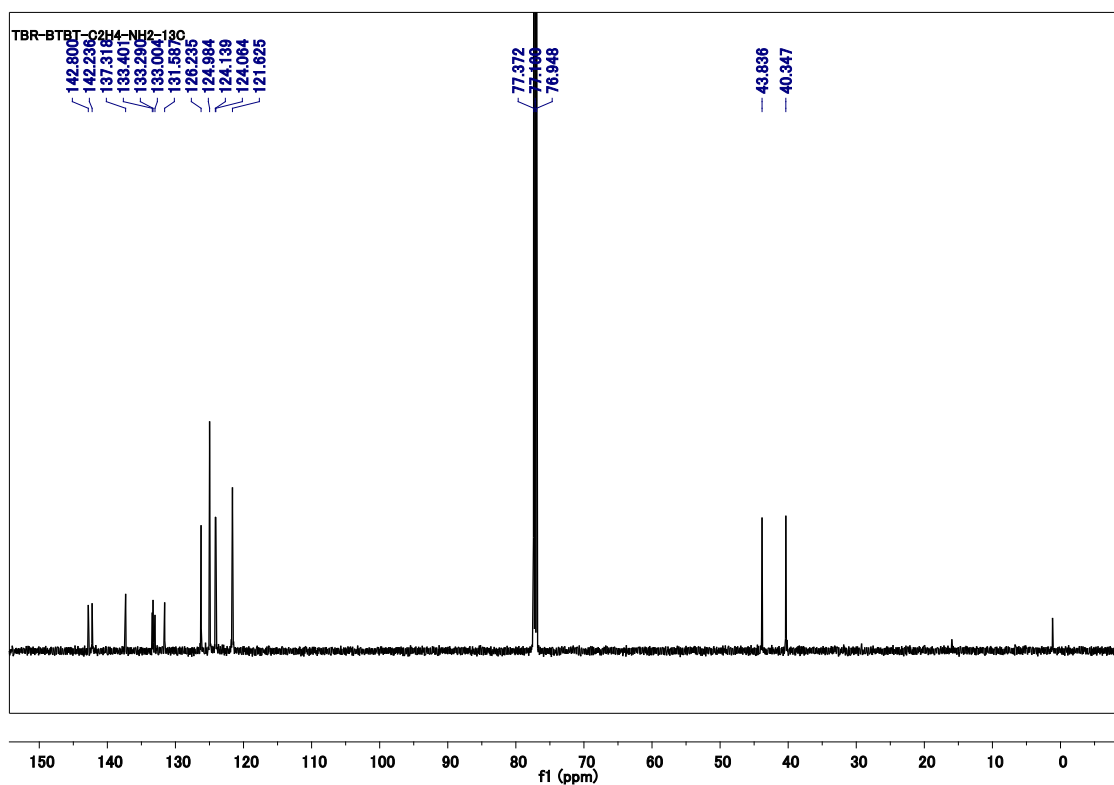


Figure S11. ^{13}C NMR spectrum of V in deuterated chloroform.

Fig

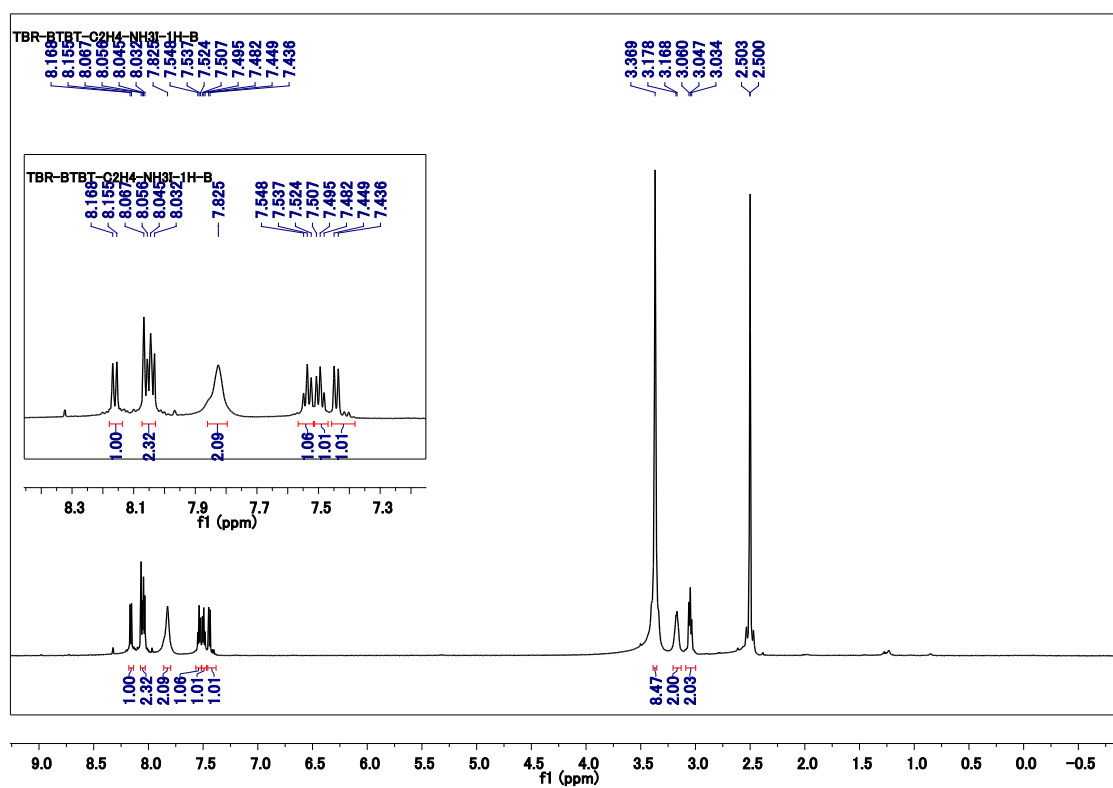


Figure S12. ^1H NMR spectrum of VI in deuterated DMSO.

Fi

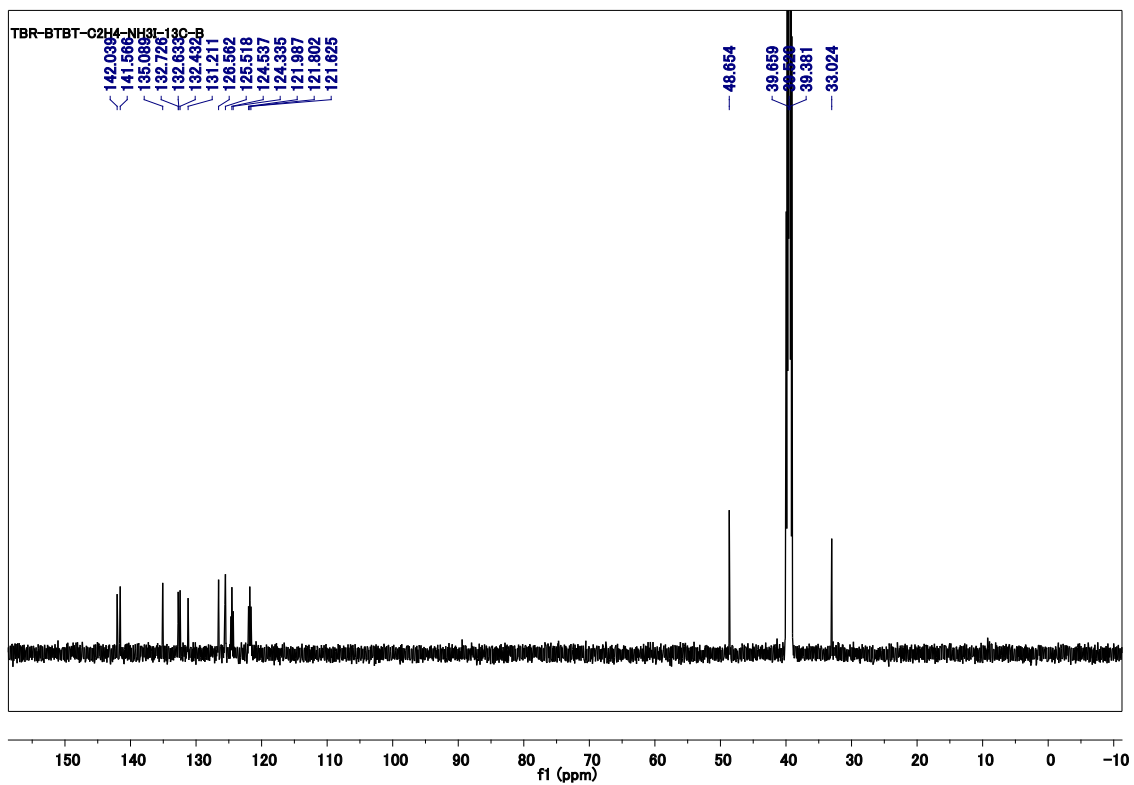


Figure S13. ^{13}C NMR spectrum of VI in deuterated DMSO.

Table S1. Summary of the mean values and standard deviation of J_{SC} , V_{OC} , FF, and PCE for mixed cation-based PSCs treated with BTBTAI solutions at various concentrations.

BTBTAI solution concentration (mM)	J_{SC} (mA cm⁻²)	V_{OC} (V)	FF	PCE (%)
0 (untreated)	23.9 ± 0.2	1.04 ± 0.01	0.68 ± 0.01	17.6 ± 0.2
0.01	24.2 ± 0.1	1.08 ± 0.01	0.69 ± 0.01	18.0 ± 0.3
0.05	23.5 ± 0.7	1.08 ± 0.01	0.71 ± 0.01	18.0 ± 0.5
0.1	24.1 ± 0.1	1.08 ± 0.01	0.70 ± 0.01	18.3 ± 0.2
0.5	24.6 ± 0.1	1.09 ± 0.01	0.71 ± 0.01	19.1 ± 0.3
1	24.8 ± 0.3	1.10 ± 0.01	0.75 ± 0.01	20.2 ± 0.2
1.5	25.6 ± 0.3	1.11 ± 0.01	0.73 ± 0.01	20.7 ± 0.1
2	26.9 ± 0.3	1.08 ± 0.01	0.72 ± 0.01	20.9 ± 0.4

Table S2. Summary of the mean values and standard deviation of J_{SC} , V_{OC} , FF, and PCE for mixed cation-based PSCs treated with 1 mM solutions of PEAI, NMAI, AMAI, and BTBTAI.

Treatment material	J_{SC} (mA cm⁻²)	V_{OC} (V)	FF	PCE (%)
Reference (untreated)	23.9 ± 0.2	1.04 ± 0.01	0.68 ± 0.01	17.6 ± 0.2
PEAI	24.1 ± 0.3	1.06 ± 0.01	0.71 ± 0.01	18.2 ± 0.2
NAMI	24.3 ± 0.2	1.07 ± 0.01	0.74 ± 0.01	19.2 ± 0.2
AMAI	24.6 ± 0.4	1.08 ± 0.01	0.75 ± 0.01	19.9 ± 0.3
BTBTAI	24.8 ± 0.3	1.10 ± 0.01	0.75 ± 0.01	20.2 ± 0.2

Table S3. Summary of the mean values and standard deviation of J_{SC} , V_{OC} , FF, and PCE for mixed cation-based PSCs treated with PEAI solutions at various concentrations.

PEAI solution concentration (mM)	J_{SC} (mA cm⁻²)	V_{OC} (V)	FF	PCE (%)
0 (untreated)	23.9 ± 0.2	1.04 ± 0.01	0.68 ± 0.01	17.6 ± 0.2
0.5	24.0 ± 0.2	1.05 ± 0.01	0.68 ± 0.01	17.9 ± 0.2
1	24.1 ± 0.3	1.06 ± 0.01	0.71 ± 0.01	18.2 ± 0.2
2	24.2 ± 0.2	1.06 ± 0.01	0.71 ± 0.01	18.4 ± 0.3
3	24.3 ± 0.2	1.07 ± 0.01	0.71 ± 0.01	18.4 ± 0.3
4	24.0 ± 0.2	1.07 ± 0.01	0.71 ± 0.01	18.0 ± 0.3
5	23.8 ± 0.2	1.06 ± 0.01	0.70 ± 0.01	17.6 ± 0.2
10	23.1 ± 0.3	1.04 ± 0.01	0.69 ± 0.01	16.5 ± 0.4

Table S4. Summary of the mean values and standard deviation of J_{SC} , V_{OC} , FF, and PCE for FAPbI₃-based PSCs both untreated and treated with BTBTAI.

Treatment material	J_{SC} (mA cm⁻²)	V_{OC} (V)	FF	PCE (%)
Reference (untreated)	25.9 ± 0.2	1.09 ± 0.01	0.81 ± 0.01	22.7 ± 0.6
BTBTAI	26.1 ± 0.2	1.14 ± 0.01	0.83 ± 0.01	24.6 ± 0.5

Table S5. Summary of the TPV lifetimes for FAPbI₃-based PSCs, both untreated and treated with BTBTAI. TPV decay curves were measured before (τ_0) and after (τ) the operational durability test. The TPV lifetimes were estimated as the time required for the voltage to decay to 1/e of its original value, based on Figure 6(e). Compared to untreated PSCs, the smaller decrease in τ/τ_0 observed in BTBTAI-treated PSCs indicates that the BTBTAI treatment effectively suppresses the enhanced carrier recombination caused by degradation.

Treatment material	τ_0 (ms)	τ (ms)	τ/τ_0
Reference (untreated)	58.7	2.24	0.0382
BTBTAI	124	80.3	0.648

Table S6. Summary of the TPC lifetimes for FAPbI₃-based PSCs, both untreated and treated with BTBTAI. TPC decay curves were measured before (τ_0) and after (τ) the operational durability test. The TPC lifetimes were estimated as the time required for the current to decay to 1/e of its original value, based on Figure 6(f). Compared to untreated PSCs, the smaller increase in τ/τ_0 observed in BTBTAI-treated PSCs indicates that the decline in hole extraction due to degradation is effectively suppressed by the BTBTAI treatment.

Treatment material	τ_0 (μ s)	τ (μ s)	τ/τ_0
Reference (untreated)	2.56	3.55	1.39
BTBTAI	1.98	2.38	1.20

Table S7. Summary of the mean values and standard deviation of J_{SC} , V_{OC} , FF, and PCE for inverted PSCs both untreated and treated with BTBTAI.

Treatment material	J_{SC} (mA cm ⁻²)	V_{OC} (V)	FF	PCE (%)
Reference (untreated)	22.0 ± 0.5	1.19 ± 0.01	0.79 ± 0.01	20.8 ± 0.4
BTBTAI	20.1 ± 0.7	1.03 ± 0.07	0.44 ± 0.03	9.2 ± 1.0

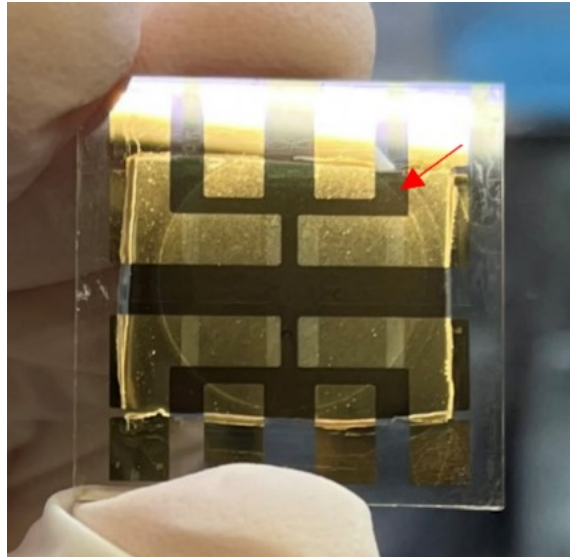


Figure S14. Photograph of a mixed cation-based PSC treated with a 2 mM BTBTAI solution. The red arrow highlights the circular-shaped thick crystalline BTBTAI precipitate formed on the perovskite layer.

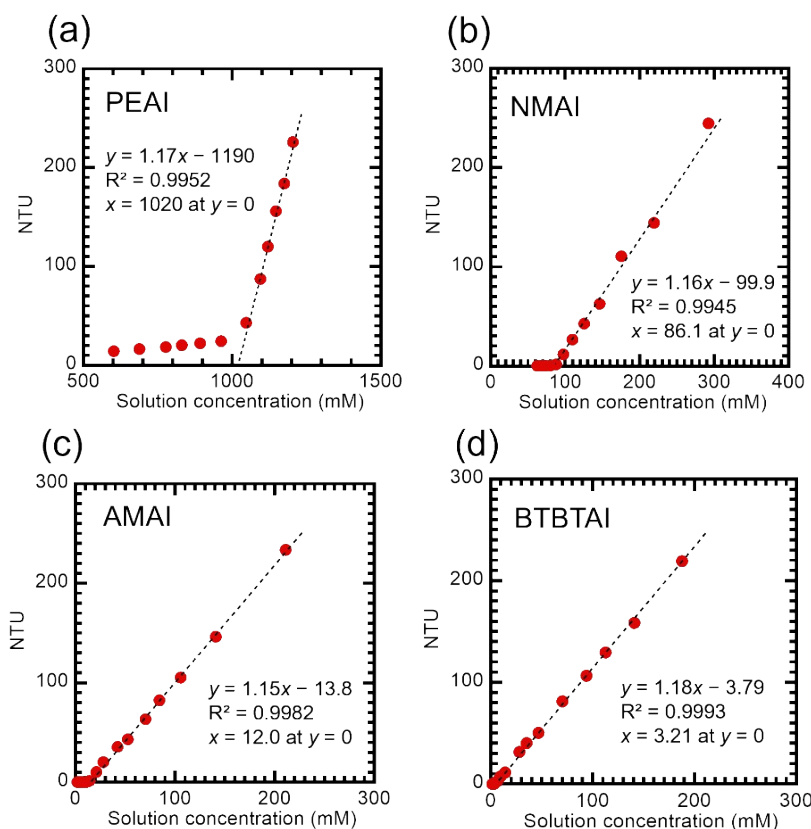


Figure S15. Turbidity measurements of (a) PEAI, (b) NMAI, (c) AMAI, and (d) BTBTAI solutions (EtOH) at varying concentrations were performed using a lab-made turbidimeter. Collimated 780 nm NIR laser (CPS780S, Thorlabs) was directed into a fused silica cuvette containing the solution, with each powder thoroughly ground prior to solution preparation. During the measurements, the solutions were stirred to prevent undissolved powder from settling at the bottom of the cuvette. The transmitted light intensity (I_{\parallel}) was measured with a power meter (PM16-120, Thorlabs) along the direction of light incidence, while the scattered light intensity (I_{\perp}), indicative of solution turbidity caused by undissolved powder, was measured at a perpendicular angle using another power meter. As solutions' turbidity increased, I_{\parallel} decreased and I_{\perp} increased, with the I_{\perp}/I_{\parallel} ratios proportional to the amount of undissolved powder in the solutions. Turbidity values, expressed in nephelometric turbidity units (NTU), were calibrated using commercially available standards. At lower concentrations of NMAI, AMAI, and BTBTAI solutions, NTU values were zero, indicating complete dissolution of the passivation materials in EtOH. As concentrations of these solutions increased, NTU values rose rapidly, reflecting a higher presence of undissolved material. For PEAI solutions, however, NTU values were not zero even at lower concentrations below approximately 1,000 mM, before the rapid NTU rise. This was likely due to PEAI sol formation at high concentrations. Despite the absence of undissolved PEAI, cloudiness caused by the sol was observed in the cuvette, leading to light scattering by the sol and resulting in non-zero NTU values. In this region, NTU values decreased as concentrations were reduced, possibly due to sol dissociation. By fitting the NTU plots and defining the intersection with the x -axis as the solubility, solubility was estimated to be approximately 1,020 mM for PEAI, 86.1 mM for NMAI, 12.0 mM for AMAI, and 3.21 mM for BTBTAI. As expected, materials with larger molecular weights (extended π -conjugation) exhibited lower solubility.

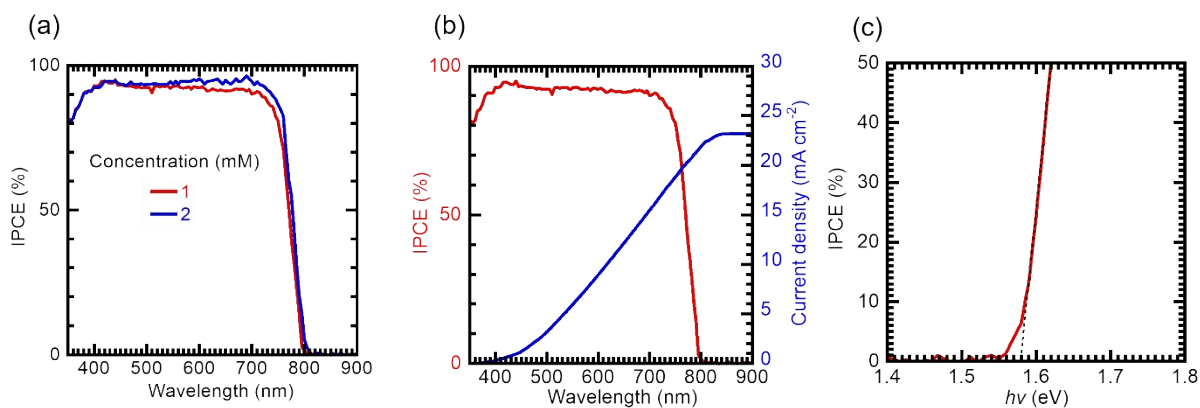


Figure S16. (a) IPCE curves of mixed-cation-based PSCs treated with 2 mM and 1 mM BTBTAI solutions. (b) IPCE curve and corresponding integrated current density of a mixed-cation-based PSC treated with a 1 mM BTBTAI solution. The red curves in (a) and (b) are identical. (c) IPCE curve from (b) plotted with the x-axis in energy (eV) instead of wavelength.

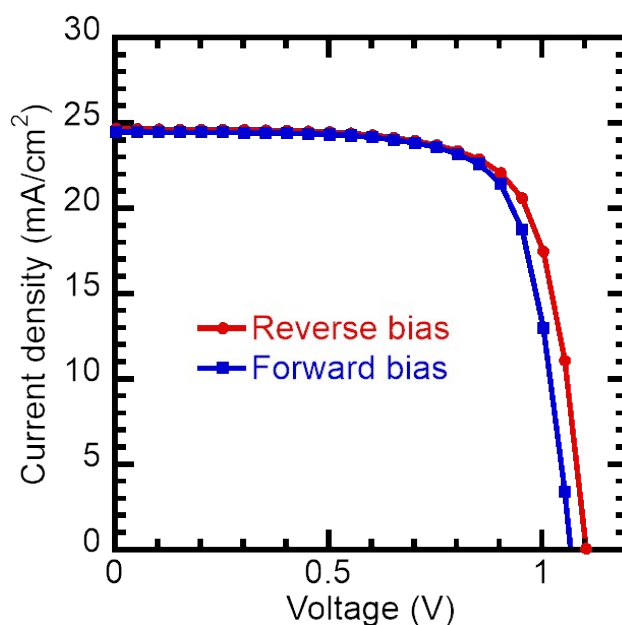


Figure S17. Illuminated J - V curves of mixed cation-based PSCs treated with a 1 mM BTBTAI solution. In the forward scan (0 V to 1.2 V), PCE = 19.3%, J_{SC} = 24.5 mA cm⁻², V_{OC} = 1.06 V, and FF = 0.740. In the reverse scan (1.2 V to 0 V), PCE = 19.9%, J_{SC} = 24.6 mA cm⁻², V_{OC} = 1.10 V, and FF = 0.741.

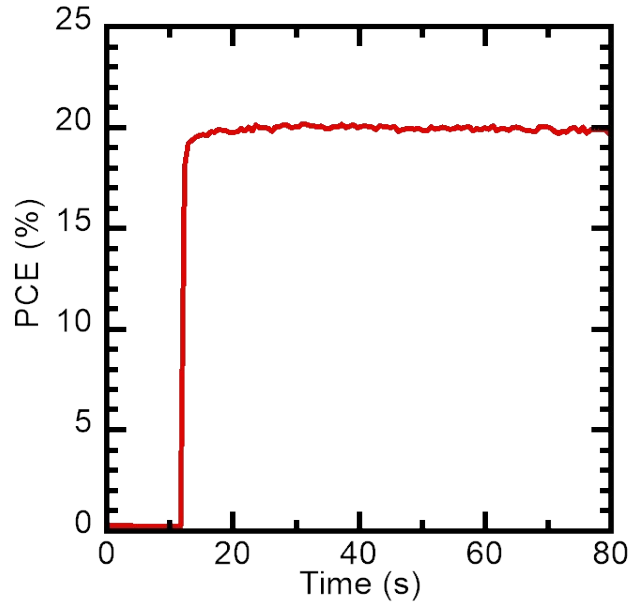


Figure S18. MPPT operation of a mixed cation-based PSC to evaluate PCE stabilization under the simulated one-sun illumination.

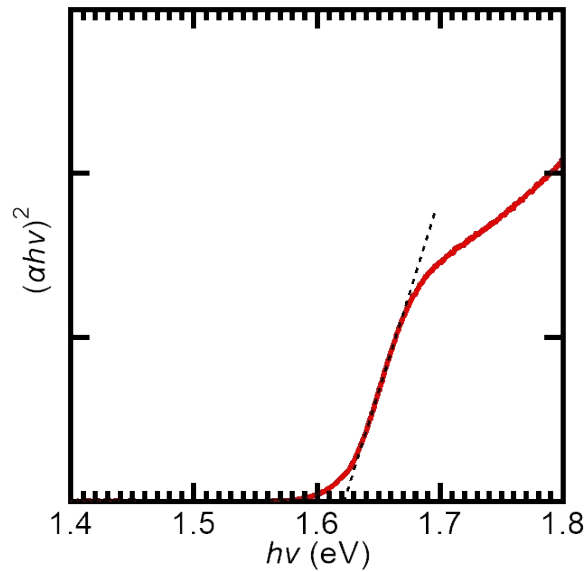


Figure S19. Tauc plot for a mixed cation-based perovskite film fabricated on a fused silica substrate. The absorption spectrum was measured using a spectrometer equipped with an integrating sphere to minimize the effects of light scattering and interference, allowing for a clearer observation of the absorption onset. The optical bandgap calculated from the Tauc plot was 1.62 eV.

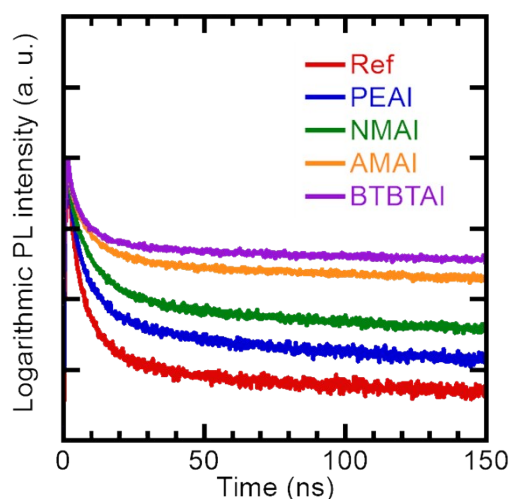


Figure S20. Time-resolved transient PL decays of untreated mixed cation-based perovskite films and those treated with PEAI, NMAI, AMAI, and BTBTAI. These samples were rinsed by spin-coting with CB before the measurements. The initial fast decays are likely due to defect-induced nonradiative carrier recombination, while the slower decays may correspond to intrinsic radiative carrier recombination. The intensity of the slower decay components increases with surface treatment due to defect passivation.

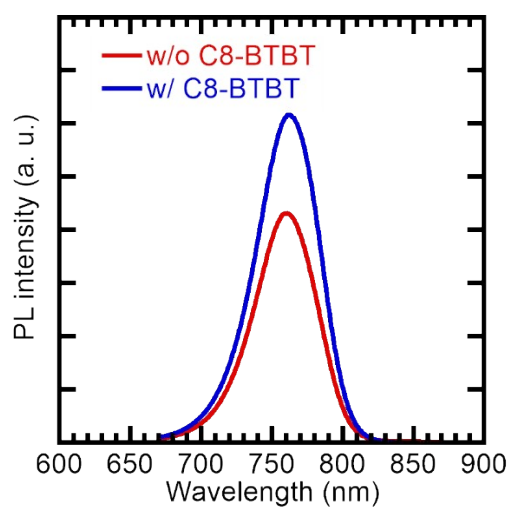


Figure S21. Steady-state PL spectra of mixed cation-based perovskite films without and with C8-BTBT.

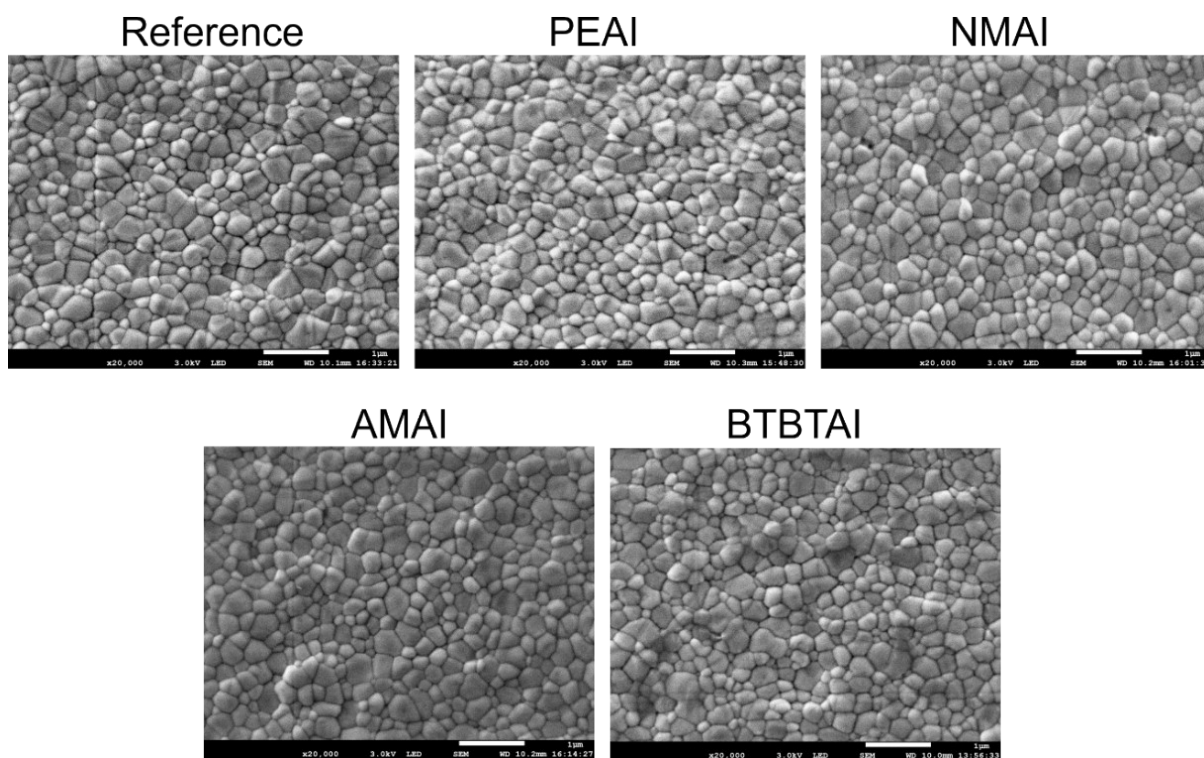


Figure S22. SEM images of untreated mixed cation-based perovskite films and those treated with PEAI, NMAI, AMAI, and BTBTAI. The white scale bars in each image represent 1 μm .

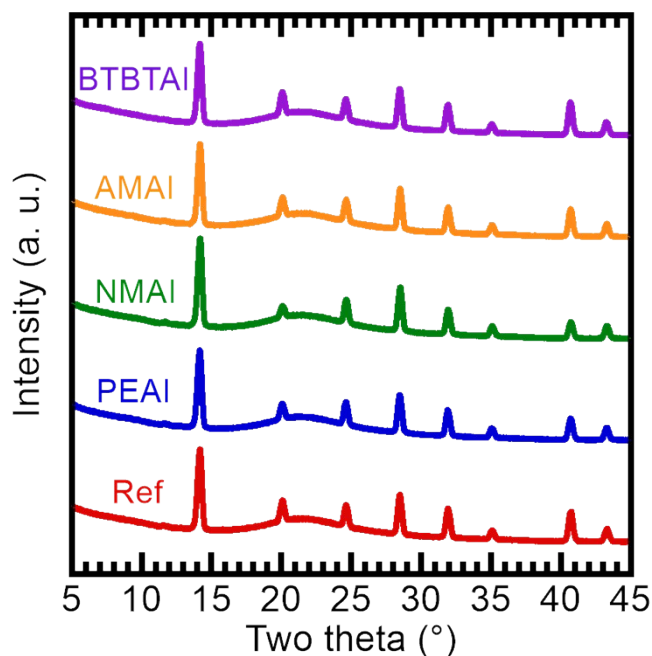


Figure S23. XRD patterns of untreated mixed cation-based perovskite films and those treated with PEAI, NMAI, AMAI, and BTBTAI. The broad peaks centered around 20° in the diffraction patterns reflect the amorphous nature of the glass substrates.

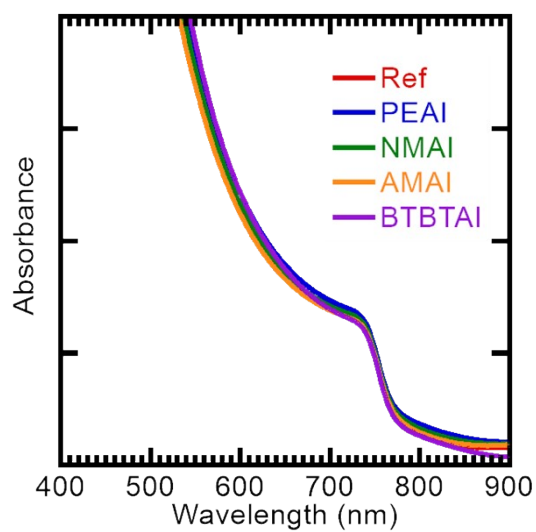


Figure S24. UV-VIS absorption spectra of untreated mixed cation-based perovskite films and those treated with PEAI, NMAI, AMAI, and BTBTAl.

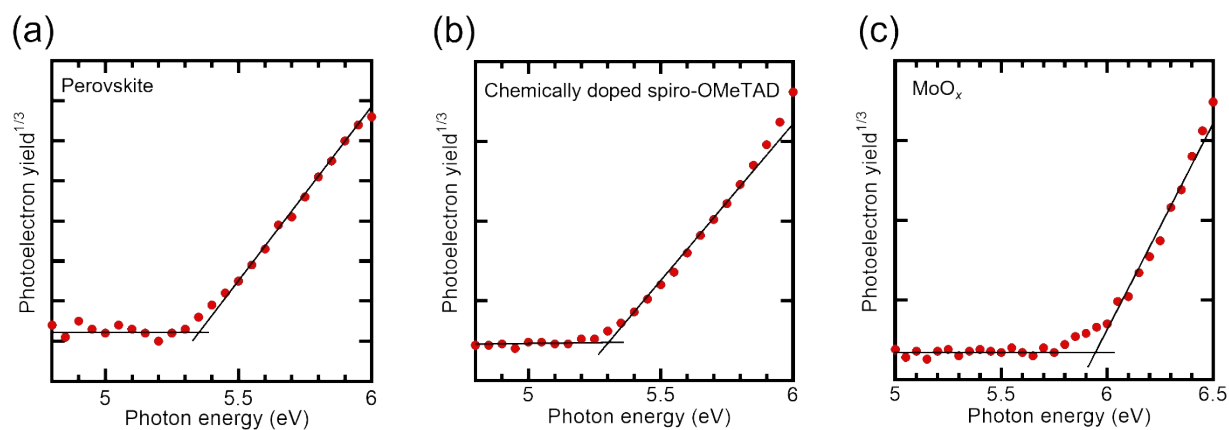


Figure S25. PYS plots of (a) mixed cation-based perovskite, chemically doped spiro-OMeTAD, and MoO_x films fabricated on ITO-coated glass substrates.

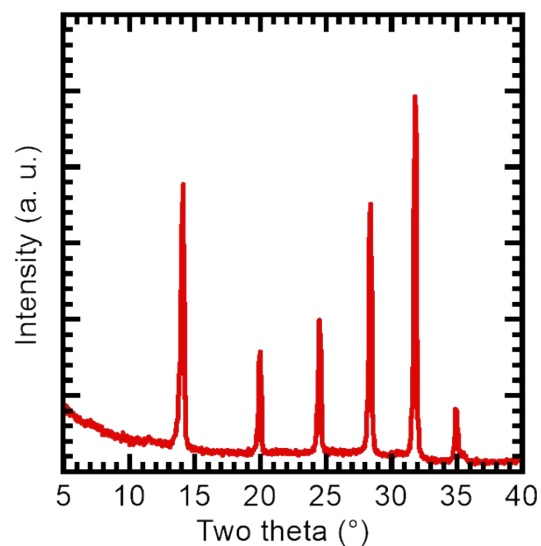


Figure S26. GIXRD pattern of BTBTAI-treated mixed cation-based perovskite films. The 3D perovskite phase was clearly detected, while the lower-dimensional perovskite phase was absent, consistent with the standard XRD results shown in Figure S23†.

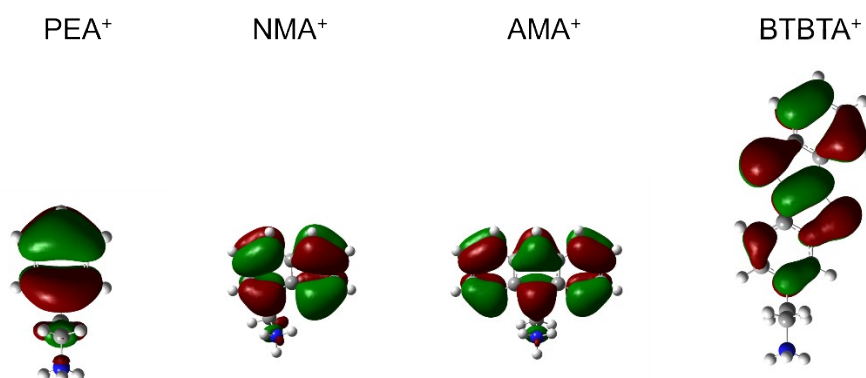


Figure S27. Optimized molecular structures and corresponding HOMO orbitals of PEA⁺, NMA⁺, AMA⁺, and BTBTA⁺.